Syntheses of Reactive Mixed-Metal Carbide Clusters and Their Interaction with Proton Sources†

Joseph A. Hriljac, Paul N. Swepston, and Duward F. Shriver*

Department of Chemistry, Northwestern University, Evanston, Illinois 60201

Received July 2, 1984

The three-iron ketenylidene $[Fe_3(CO)_9(CCO)]^{2-}$, I, undergoes a redox condensation reaction with $[Rh(CO)_2Cl]_2$ to produce a reactive butterfly carbide $[RhFe_3(CO)_{12}C]^-$, VIII. Similarly, I in the prescence of $[Mn(CO)_5(CH_3CN)]^+$ leads to $[MnFe_3(CO)_{13}C]^-$, IX. Both products were characterized by ^{13}C NMR spectroscopy, and the structure of the rhodium cluster VIII was determined by single-crystal X-ray diffraction. Monoprotonation of VIII and IX yields the butterfly methylidynes $RhFe_3(CO)_{12}(CH)$, XII, and $MnFe_3(CO)_{13}(CH)$, XIII. This site of protonation contrasts with the butterfly carbide $[Fe_4(CO)_{12}C]^{2-}$, II, which first protonates on the metal framework. In some cases the redox condensation reaction does not terminate at the four-metal butterfly cluster stage, thus the reaction of I with $[CpNi(CO)]_2$ yields $[Ni_3Fe_3(CO)_{13}C]^{2-}$, X. Attempts to generate a butterfly carbide via a metal substitution pathway employing II and $Co_2(CO)_8$ did not lead to a tetranuclear cluster but produced instead the pentanuclear carbide $[CoFe_4(CO)_{14}C]^-$, XI, the structure of which was also determined by single-crystal X-ray diffraction. X-ray crystal data for $[PPN][RhFe_3(CO)_{12}C]\cdot CH_2Cl_2$, VIII: orthorhombic, a = 17.780 (2) Å, b = 19.641 (4) Å, c = 15.145 (4) Å, Z = 4, space group $Pna2_1$. For $[PPN][CoFe_4(CO)_{14}C]$, XI: monoclinic, a = 17.403 (3) Å, b = 16.030 (3) Å, c = 19.055 (2) Å, β = 105.34 (1)°, Z = 4, space group $P2_1/n$.

Introduction

Recently the reactive ketenylidene cluster $[Fe_3(CO)_9(CCO)]^{2-}$, I, was synthesized in high yield via the reductive cleavage of carbon monoxide (eq 1).[1] This cluster displays

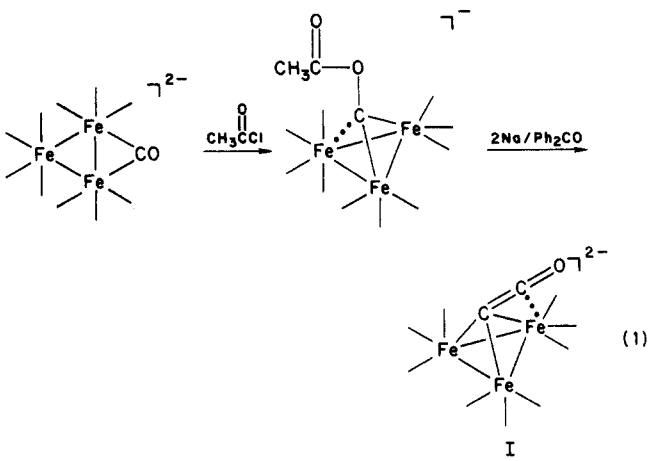

(1)

I

reactions with electrophiles such as acids and methylating agents at the α-carbon of the ketenyl moiety to yield methylidyne or ethylidyne derivatives, with migration of the ketenyl carbonyl onto the metal framework (eq 2).[2]

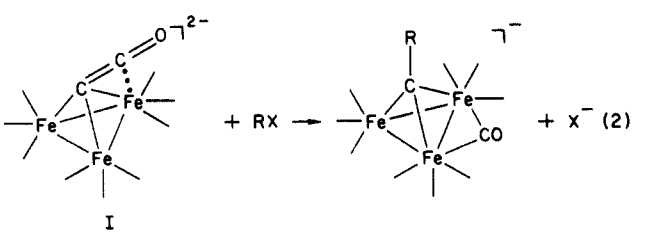

(2)

I

R = H, Me

Reactivity at the carbide ligand is also known for the isoelectronic series of tetranuclear butterfly compounds $[Fe_4(CO)_{12}C]^{2-}$, II,[3] $[HFe_4(CO)_{12}C]^-$, III,[3,4] and $Fe_4(CO)_{13}C$, IV,[5] but not for any higher nuclearity carbide cluster. These data indicate that the carbide ligand is reactive only when it is in the exposed environment of a low-nuclearity cluster.[1,6]

Earlier work in Muetterties' laboratory demonstrated the utility of the carbide clusters II and $[Fe_5(CO)_{14}C]^{2-}$ in redox condensation cluster building reactions to yield pentanuclear and hexanuclear carbide clusters.[7] In a preliminary communication, we reported the utilization of the ketenylidene cluster I in redox condensation reactions to generate the first mixed-metal butterfly carbide clusters $[MFe_3(CO)_{13}C]^{2-}$ (M = Cr, W; VIa,b) (eq 3).[8]

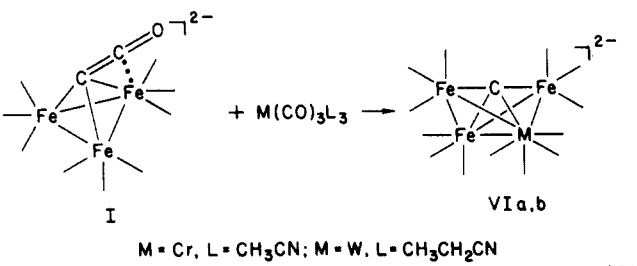

I VIa,b

M = Cr, L = CH3CN; M = W, L = CH3CH2CN

(3)

Analogous to the homometallic II, these mixed-metal butterfly carbides display reactivity at the carbide ligand. For example, the methylidyne cluster $HWFe_3(CO)_{13}(CH)$, VII, is produced by the reaction of VIb with 2 equivalents of acid.[8]

In the present report we describe the syntheses of two new mixed-metal butterfly carbides and their reactivity with acids to generate new methylidyne clusters. We also

†This manuscript is dedicated to the memory of E. L. Muetterties, a friend and a leader in inorganic chemistry.

(1) Kolis, J. W.; Holt, E. M.; Drezdzon, M.; Whitmire, K. H.; Shriver, D. F. *J. Am. Chem. Soc.* **1982**, *104*, 6134.
(2) Kolis, J. W.; Holt, E. M.; Shriver, D. F. *J. Am. Chem. Soc.* **1983**, *105*, 7307.
(3) (a) Tachikawa, M.; Muetterties, E. L. *J. Am. Chem. Soc.* **1980**, *102*, 4541. (b) Davis, J. H.; Beno, M. A.; Williams, J. M.; Zimmie, J.; Tachikawa, M.; Muetterties, E. L. *Proc. Natl. Acad. Sci. U.S.A.* **1981**, *78*, 668.
(4) Holt, E. M.; Whitmire, K. H.; Shriver, D. F. *J. Organomet. Chem.* **1981**, *213*, 125.
(5) (a) Bradley, J. S.; Ansell, G. B.; Leonowicz, M. E.; Hill, E. W. *J. Am. Chem. Soc.* **1981**, *103*, 4968. (b) Bradley, J. S. *Philos. Trans. R. Soc. London A* **1982**, *308*, 103.
(6) (a) Tachikawa, M.; Muetterties, E. L. *Prog. Inorg. Chem.* **1981**, *28*, 203. (b) Bradley, J. S. *Adv. Organomet. Chem.* **1983**, *22*, 1.
(7) (a) Tachikawa, M.; Sievert, A. C.; Muetterties, E. L.; Thompson, M. R.; Day, C. S.; Day, V. W. *J. Am. Chem. Soc.* **1980**, *102*, 1725. (b) Tachikawa, M.; Geerts, R. L.; Muetterties, E. L. *J. Organomet. Chem.* **1981**, *213*, 11.
(8) Kolis, J. W.; Holt, E. M.; Hriljac, J. A.; Shriver, D. F. *Organometallics* **1984**, *3*, 496.

0276-7333/85/2304-0158$01.50/0

report the syntheses of two new higher nuclearity clusters and discussed the general synthetic pathways for generating tetranuclear mixed-metal butterfly carbides.

Experimental Section

General Procedures. All manipulations were carried out under a purified nitrogen atmosphere using standard Schlenk and needlestock techniques or in a Vacuum Atmospheres drybox. THF, Et_2O, and pentane were distilled from sodium benzophenone ketyl under nitrogen. Methylene chloride was distilled from P_2O_5 under nitrogen. 2-Propanol and MeOH were distilled from Mg/I_2, and acetonitrile was degassed before use. CD_2Cl_2 (99.3 atom % D, Cambridge isotopes) was vacuum distilled from P_2O_5 prior to use. IR spectra were recorded on either a Perkin-Elmer 399 or 283 spectrometer using 0.1-mm path length CaF_2 solution cells or as Nujol mulls between KBr plates. ^1H and ^{13}C NMR spectra were recorded on a JEOL-FX270 spectrometer operating at 269.65 and 67.8 MHz, respectively. All chemical shifts are reported positive if downfield relative to Me_4Si and are referenced indirectly to Me_4Si, using residual solvent protons (^1H) or the solvent (^{13}C) as internal references. ^{13}C NMR spectra were typically recorded with $Cr(acac)_3$ as a relaxation agent, but in most cases satisfactory spectra could be obtained without it. Mass spectra were obtained by Dr. D. Hung of the Northwestern University Analytical Services Laboratory on a HP5985A spectrometer using 70-eV ionization and analyzed by using MASPAN.[9] The PPN+ and Ph_4P^+ salts of $[Fe_3(CO)_9(CCO)]^{2-}$, I,[2] $[CpNi(CO)]_2$,[10] $[Rh(CO)_2Cl]_2$,[11] and $[Mn(CO)_5(CH_3CN)][PF_6]$[12] were prepared by literature procedures. $Co_2(CO)_8$ (Strem) was sublimed prior to use. The ^{13}C-enriched compounds were prepared by starting from I that was enriched to ca. 20% at all 11 carbons.[2] Elemental analyses were performed by Galbraith Laboratories.

$[PPN][RhFe_3(CO)_{12}C]\cdot CH_2Cl_2$, VIII. A 0.67-g (0.44-mmol) sample of $[PPN]_2[Fe_3(CO)_9(CCO)]$ and 0.17 g (0.44 mmol) of $[Rh(CO)_2Cl]_2$ were dissolved in 10 mL of CH_2Cl_2. After 10 min of stirring 50 mL of Et_2O was added and the red-brown solution was separated by filtration from solid $[PPN][Rh(CO)_2Cl_2]$. The solution was concentrated to ca. 50 mL, and 30 mL of pentane was added with rapid stirring. The cloudy solution was cooled to −10 °C, and after 12 h the dark red-black crystals were collected by filtration and washed with pentane: isolated 0.22 g (43% yield); IR ν_{CO} (CH_2Cl_2) 2074 (w), 2017 (vs), 1979 (s), 1962 (m), 1944 (w, sh) cm^{-1}; IR ν_{CO} (Nujol) 2075 (m), 2018 (sh), 2003 (s), 1986 (sh), 1977 (s), 1957 (s), 1949 (s), 1939 (s), 1922 (s), 1910 (s) cm^{-1}; ^{13}C NMR (CD_2Cl_2, −50 °C) 461.1 (d, $^1J_{Rh-C}$ = 19.5 Hz), 218.0 (s), 215.9 (s), 190.4 (d, $^1J_{Rh-C}$ = 63.5 Hz) ppm (ca. intensities 1:3:6:3). Anal. Calcd for $C_{50}H_{32}Cl_2Fe_3NO_{12}P_2Rh$: C, 48.34; H, 2.60; N, 1.13; Fe, 13.49; Rh, 8.28. Found: N, 1.04; Fe, 11.13; Rh, 9.54 (on a separate sample, C, 49.05; H, 2.81; Fe, 12.35; Rh, 8.49).

$[Ph_4P][MnFe_3(CO)_{13}C]$, IX. A 1.00-g (0.879-mmol) sample of $[Ph_4P]_2[Fe_3(CO)_9(CCO)]$ and 0.33 g (0.87 mmol) of $[Mn(CO)_5(CH_3CN)][PF_6]$ were slurried in 20 mL of CH_2Cl_2. The reaction was monitored by IR spectroscopy, and after 24 h of stirring the bands at 1924 and 1872 cm^{-1}, associated with the iron starting material, disappeared and product bands formed. A 70-mL sample of Et_2O was added to the green-brown solution, and the resulting precipitate of $[Ph_4P][PF_6]$ was removed by filtration. The solvent was removed in vacuo, the green-black solids were extracted with 40 mL of 2-propanol and filtered, and 30 mL of pentane was added to the filtrate. The solution was cooled to −10 °C, and after 24 h the black microcrystals were collected by filtration and washed with pentane: isolated 0.36 g (45% yield); IR ν_{CO} (CH_2Cl_2) 2018 (sh), 2008 (s), 1990 (s), 1967 (sh), 1947 (sh), 1770 (w, br) cm^{-1}; IR ν_{CO} (Nujol) 1992 (vs), 1956 (s), 1940 (s,sh), 1925 (m,sh), 1896 (m), 1845 (w), 1779 (w, br) cm^{-1}. Anal. Calcd for $C_{38}H_{20}Fe_3MnO_{13}P$: C, 48.65; H, 2.15; P, 3.30; Fe, 17.86; Mn, 5.86. Found: C, 50.94; H, 2.21; P, 3.31; Fe, 17.69; Mn, 4.33 (on a separate sample, C, 49.76; H, 2.21; Mn, 4.04).

$[PPN][MnFe_3(CO)_{13}C]$. This was prepared in an analogous fashion to IX, except crystals were obtained by cooling a MeOH solution instead of a 2-propanol/pentane solution: isolated 0.14 g (19% yield); IR ν_{CO} (CH_2Cl_2) 2019 (sh), 2008 (s), 1989 (s), 1962 (sh), 1940 (sh), 1858 (w, br), 1771 (w, br) cm^{-1}; ^{13}C NMR (CD_2Cl_2, −80 °C) 468.4 (s), 237.5 (s), 224.1 (s), 215.0 (s), 214.0 (s), 208.7 (s) ppm (ca. intensities: 1:0.5:1:6:1:1). Anal. Calcd for $C_{50}H_{30}Fe_3MnNO_{13}P_2$: N, 1.23; Fe, 14.73; Mn, 4.83. Found: N, 1.31; Fe, 14.16; Mn 3.86.

$[MnFe_3(CO)_{13}(CH)]$, XIII. A 0.10-g (0.11-mmol) sample of IX was dissolved in 5 mL of CH_2Cl_2, and 25 μL (0.27 mmol) of HSO_3CF_3 was added with rapid stirring. After 30 min of rapid stirring, the red-brown solution was evaporated to dryness and the resulting solids were extracted with 15 mL of pentane, filtered, and concentrated to ca. 5 mL. Upon cooling to −10 °C for 1 day black needles had formed. These were collected by filtration and dried in vacuo: isolated 0.035 g (53% yield); IR ν_{CO} (C_6H_{12}) 2053 (vs), 2035 (sh), 2027 (s), 2013 (sh), 1997 (m), 1979 (w, sh), 1914 (m) cm^{-1}; ^1H NMR (CD_2Cl_2, +20 °C) −0.33 ppm; ^{13}C NMR (CD_2Cl_2, −90 °C) 335.5 (d, $^1J_{C-H}$ = 107.4 Hz), 224.5 (s), 222.4 (s), 218.6 (s), 210.0 (s), 209.6 (s), 207.3 (s), 206.8 (s), 204.4 (s) ppm (ca. intensities 1:1:1:2:2:2:2:2:1); mass spectrum, parent ion at m/e 600 with loss of 13 CO's down to the Fe_3MnCH^+ core; isotopic fit to parent ion, R = 16.6% with no hydrogen loss; isotopic fit to core, R = 24.5% with no hydrogen loss and R = 9.1% with 12% hydrogen loss.

$[PPN]_2[Ni_3Fe_3(CO)_{13}C]$, X. A 1.30-g (0.848-mmol) sample of $[PPN]_2[Fe_3(CO)_9(CCO)]$ and 0.80 g (2.6 mmol) of $[CpNi(CO)]_2$ were slurried in 40 mL of CH_3CN. The reaction was monitored by IR spectroscopy and after 2 days of stirring the bands of the iron starting material had disappeared. The dark green-black solution was evaporated to dryness, and the solids were extracted with 20 mL of THF. The solution was cooled to 0 °C and filtered to remove any unreacted I. The THF was removed in vacuo, the solids were dissolved in 12 mL of CH_2Cl_2, and this solution was layered with 25 mL of Et_2O. After diffusion was complete, the resulting black crystals were collected by filtration and washed with Et_2O: isolated 1.24 g (81% yield based on the iron starting material); IR ν_{CO} (CH_2Cl_2) 1980 (sh), 1977 (s), 1964 (sh), 1934 (m), 1885 (w, sh), 1820 (w, br) cm^{-1}; IR ν_{CO} (THF) 1981 (sh), 1971 (s), 1955 (s), 1926 (m), 1887 (w), 1825 (w, br) cm^{-1}; IR ν_{CO} (Nujol) 2017 (w), 1972 (s), 1959 (s), 1912 (s), 1881 (m, sh), 1827 (w, sh), 1810 (m) cm^{-1}; ^{13}C NMR (CD_2Cl_2, −90 °C) 435.1 (s), 243.4 (s), 226.2 (s), 197.3 (s) ppm (ca. intensities 1:1:7:3). Anal. Calcd for $C_{86}H_{60}Fe_3N_2Ni_3O_{13}P_4$: C, 57.48; H, 3.37; N, 1.56; Fe, 9.32; Ni, 9.80. Found: C, 54.64; H, 3.35; N, 1.57; Fe, 9.78; Ni, 7.79 (on a separate sample, N, 1.54; Fe, 9.05; Ni, 8.27).[13]

$[PPN][CoFe_4(CO)_{14}C]$, XI. A 1.02-g (0.619-mmol) sample of $[PPN]_2[Fe_3(CO)_9(CCO)]$ and 0.21 g (0.61 mmol) of $Co_2(CO)_8$ were dissolved in 10 mL of CH_2Cl_2. After 10 min of stirring the red-brown solution was evaporated to dryness. The oily black solids were extracted with 20 mL of Et_2O and filtered, and 20 mL of pentane was added with rapid stirring. The red-black microcrystals were collected by filtration and washed with pentane: isolated 0.49 g (65% yield); IR ν_{CO} (CH_2Cl_2) 2064 (w), 2015 (sh), 1999 (vs), 1822 (w, br) cm^{-1}; IR ν_{CO} (Et_2O) 2064 (w), 2014 (s), 1999 (vs), 1822 (w, br) cm^{-1}; IR ν_{CO} (Nujol) 2068 (w), 2016 (sh), 1999 (vs), 1988 (sh), 1955 (s), 1933 (m), 1814 cm^{-1}; ^{13}C NMR (CD_2Cl_2, −90 °C) 476.9 (s), 216.1 (s), 214.7 (s), 209.5 (s), 197.2 (s) ppm (ca. intensities 1:4:0.5:0.5:0.5:0.5). Anal. Calcd for $C_{51}H_{30}NFe_4CoO_{14}P_2$: C, 50.00; H, 2.47; N, 1.14; Fe, 18.24; Co, 4.81. Found: C, 50.19; H, 2.53; N, 1.14; Fe, 17.94; Co, 4.55.

X-ray Crystal Structures of $[PPN][RhFe_3(CO)_{12}C]\cdot CH_2Cl_2$, VIII, and $[PPN][CoFe_4(CO)_{14}C]$, XI. Crystals of VIII suitable for analysis were grown by slowly cooling at $CH_2Cl_2/Et_2O/C_5H_{12}$ (1:2:1) solution. Crystals of XI were grown by slow diffusion of pentane into a Et_2O solution. The crystals were sealed in thin walled glass capillaries under a N_2 atmosphere and mounted on an Enraf-Nonius CAD4 diffractometer at room temperature. The unit cell dimensions (Table I) were determined during a normal alignment procedure by least-squares refinement of the setting angles of 25 independent reflections ($30° < 2\theta < 36°$) collected

(9) MASPAN computer program version 4 by M. Andrews and H. D. Kaesz, UCLA, 1977.
(10) Fischer, E. O.; Palm, C. *Chem. Ber.* **1958**, *91*, 1725.
(11) McCleverty, J. A.; Wilkinson, G. *Inorg. Synth.* **1966**, *8*, 211.
(12) Connelly, N. G.; Dahl, L. F. *J. Chem. Soc. Chem. Commun.* **1970**, 880.

(13) Poor carbon analyses were typical for this compound, and the reported value is the best obtained. A possible explanation is the formation of metal carbide species during the analytical procedure.

Table I. Crystal Structure Data for $[PPN][RhFe_3(CO)_{12}C]\cdot CH_2Cl_2$, VIII, and $[PPN][CoFe_4(CO)_{14}C]$, XI

	VIII	XI
formula	$C_{50}H_{32}Cl_2Fe_3NO_{12}P_2Rh$	$C_{51}H_{30}CoFe_4NO_{14}P_2$
mol wt	1242.1	1225.1
cryst size, mm	ca. 0.3 × 0.3 × 0.4	ca. 0.2 × 0.2 × 0.3
cryst color	red-black	black
cryst system	orthorhombic	monoclinic
systematic absences	h00, *h* odd; 0*k*0, *k* odd; 00*l*, *l* odd; *h*0*l*, *h* odd; 0*kl*, *k* + *l* odd	h0*l*, *h* + *l* odd; 0*k*0, *k* odd
space group	$Pna2_1$	$P2_1/n$
a, Å	17.780 (2)	17.403 (3)
b, Å	19.641 (4)	16.030 (3)
c, Å	15.145 (4)	19.055 (2)
β, deg	90	105.34 (1)
V, Å^3	5288.8	5126.2
Z	4	4
D_{calcd}, g cm^{-1}	1.560	1.587
F(000)	2488	2464
λ(Mo Kα), Å	0.710 73	0.710 73
μ(Mo Kα), cm^{-1}	13.3	15.5
2θ range, deg	3-55	3-51.5
scan mode	ω-2θ	ω-2θ
scan width, deg	$\omega = 0.8 + 0.35 \tan\theta$	$\omega = 0.8 + 0.35 \tan\theta$
scan speed range, deg min^{-1}	0.78-2.75	0.78-2.06
reflctns measd	$+h,+k,+l$	$\pm h,+k,+l$
total data	6725	10 482
unique data	6290	9783
data, $I > 3\sigma(I)$	3165	4340
no. of variables	630	658
abs correctn	empirical based on psi scan data	empirical based on psi scan data
transmissn factors	0.86-1.00	0.83-1.00
R, R_w	6.82%, 8.02%	4.18%, 3.45%
weighting scheme	$\omega = 4F^2/(\sigma(I)^2 + (0.07I)^2)$	$\omega = 4F^2/(\sigma(I)^2 + (0.02I)^2)$
esd observn of unit wt	1.588	1.364

with graphite-monochromated Mo Kα radiation. Reflections were collected by using a variable scan rate with the parameters as shown in Table I. The intensities of six standards were remeasured every 3 h, and with intensity losses of 5% for VIII and 3% for XI no corrections for decay were deemed necessary. Backgrounds were measured at each side of the scan for a total time equal to half the collection time. Data were corrected for Lorentz, polarization, and background effects.[14] Anamolous dispersion terms ($\Delta f'$, $\Delta f''$) were included for all non-hydrogen atoms.

The structure of VIII was solved by location of a heavy metal position from a Patterson function followed by the use of DIRDIF[15] and conventional Fourier techniques to locate the remaining non-hydrogen atoms. The systematic absences were consistent with either of two space groups: *Pnma* or $Pna2_1$. The lack of strong peaks on the Harker line 0*y*0 associated with the centric space group *Pnma* and the position of the cluster unit as determined by DIRDIF (no crystallographically imposed symmetry for *Pnma* and therefore $Z = 8$, yielding an unreasonable density) suggested the acentric space group $Pna2_1$ as the correct choice. This space group was confirmed by successful refinement of the model. During the refinement the thermal parameters assigned to the rhodium atom became abnormally large and those associated with the hinge position iron became abnormally small. This indicated disorder and refinement was completed with 50% occupancy of each hinge site by both Rh and Fe. After the initial refinement it also became apparent that a solvent of crystallization was present that appeared to be a methylene chloride with the carbon atom highly disordered. The chlorine atoms were successfully refined with full occupancy factors, but the carbon was not refined. Refinement of scale factor, positional parameters, and anisotropic thermal parameters for all non-hydrogen atoms was carried out and converged with $R = 6.82\%$ and $R_w = 8.02\%$.[16] The final difference Fourier showed a largest peak of 1.0 e/Å^3. The enantiomorph was changed and another refinement performed. The calculated $R_w = 8.06\%$ allowed the enantiomorph to be rejected at the 0.5% significance level.[17] A low-temperature (−125 °C) data set was collected in an attempt to improve the refinement. A crystal of ca. dimensions 0.1 × 0.1 × 0.5 mm was obtained as above and mounted directly in a N_2 cold stream on the diffractometer. A data set was collected in an identical fashion as above, except 158 Friedel pairs were included. The low-temperature data were consistent with the room-temperature structure, except the solvent disorder became worse and the refinement was abandoned. Selected bond lengths and angles are listed in Table II, and positional parameters are listed in Table III.

The structure of XI was solved by direct methods using MULTAN 11/82.[18] The positions of nine atoms were determined from an E map, and conventional Fourier techniques were used to locate the remainder of the non-hydrogen atoms. Refinements were made with the Co atom in all of the possible positions in the metal framework, but attempts to distinguish the metal identities on the basis of R_w failed. In the final refinement the Co atom was arbitrarily placed in the position found for the Rh atom in the isostructural molecule $[RhFe_4(CO)_{14}C]^-$.[7a] The phenyl hydrogens were placed at idealized positions (C–H = 0.95 Å) with fixed isotropic thermal parameters during the last two least-squares cycles but were not refined. The scale factor, positional parameters, and anisotropic thermal parameters for all non-hydrogen atoms were refined to convergence, with the final $R = 4.18\%$ and $R_w = 3.45\%$. The final difference Fourier showed no peak greater than 0.3 e/Å^3. Selected bond lengths and angles are listed in Table IV and positional parameters in Table V.

Results and Discussion

Syntheses. As shown in eq 3–5, the ketenylidene cluster $[Fe_3(CO)_9(CCO)]^{2-}$, I, serves as a useful starting material for the syntheses of new mixed-metal butterfly carbide clusters. It was found necessary to employ elec-

(14) Computations were performed on a VAX 11/730 computer using the "Structure Determine Package"; B. A. Frenz and Associates: College Station, TX (Enraf-Nonius: Delft, Holland), 1982.

(15) Beurskens, P. T.; Bosman, W. P.; Doesburg, H. M.; Van Den Harh, Th. E. M.; Peick, P. A. J.; Noordik, J. H.; Beurskens, G.; Gould, R. O.; Parthasarnthi, V. In "Conformation in Biology"; Srinivason, R., Sarma, R. H., Eds.; Alemine Press: New York, 1982; pp 389–486.

(16) Function minimized $\sum w(|F_o| - |F_c|)^2$; $R = (\sum||F_o| - |F_c||)/\sum|F_o|$; $R_w = [(\sum w(|F_o| - |F_c||^2)/\sum w|F_o|^2]^{1/2}$.

(17) Hamilton, W. C. *Acta Crystallogr.* **1965**, *18*, 502.

(18) MULTAN 11/82 by P. Main, S. J. Fiske, S. E. Hull, L. Lessinger, G. Germain, J.-P. Declercq, and M. M. Woolfson, 1982.

$$[Fe_3(CO)_9(CCO)]^{2-} + [Rh(CO)_2Cl]_2 \rightarrow$$
I

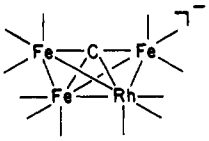

$$+ [Rh(CO)_2Cl_2]^- \quad (4)$$

VIII

$$[Fe_3(CO)_9(CCO)]^{2-} + [Mn(CO)_5(CH_3CN)]^+ \rightarrow$$
I

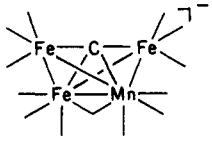

$$+ CH_3CN + 2CO \quad (5)$$

IX

trophilic transition-metal reagents that were labile or coordinatively unsaturated in these redox condensation reactions. All of the isolated clusters have been fully characterized by elemental analyses, IR spectroscopy, ^{13}C NMR spectroscopy and for $[PPN][RhFe_3(CO)_{12}C]\cdot CH_2Cl_2$, VIII, and $[PPN][CoFe_4(CO)_{14}C]$, XI, by single-crystal X-ray diffraction studies.

Reactions 4 and 5 proceed smoothly with the addition of a single heterometal fragment to $[Fe_3(CO)_9(CCO)]^{2-}$, I, to produce the mononegative clusters $[RhFe_3(CO)_{12}C]^-$, VIII, and $[MnFe_3(CO)_{13}C]^-$, IX. In contrast, the reaction of I with $[CpNi(CO)]_2$ resulted in the addition of three nickel carbonyl fragments to yield the dinegative hexanuclear cluster $[Ni_3Fe_3(CO)_{13}C]^{2-}$, X (eq 6). This product

$$[Fe_3(CO)_9(CCO)]^{2-} + 3[CpNi(CO)]_2 \rightarrow$$
I

$$[Ni_3Fe_3(CO)_{13}C]^{2-} + 3Cp_2Ni + 3CO \quad (6)$$
X

was obtained independent of the reaction solvent (THF or CH_3CN) and independent of the mole ratios of the reactants. Similarly, X was obtained when I was allowed to react with $Ni(CO)_4$ (eq 7). At some stage of reaction 6 a tetranuclear carbide cluster may be produced; however it must be more reactive than I with respect to cluster building.

$$[Fe_3(CO)_9(CCO)]^{2-} + 3Ni(CO)_4 \rightarrow$$
I

$$[Ni_3Fe_3(CO)_{13}C]^{2-} + 9CO \quad (7)$$
X

In conjunction with earlier work,[8] these results indicate that redox condensation reactions starting with $[Fe_3(CO)_9(CCO)]^{2-}$, I, provide a fairly general route to new mixed-metal butterfly carbide clusters. As illustrated by reaction 6, redox condensation may proceed beyond single metal addition. This same lack of control was observed when $[Fe_4(CO)_{12}C]^{2-}$, II, underwent the addition of two heterometal atoms to yield hexanuclear clusters.[7] The multiple metal addition reactions occur in some syntheses of dinegative carbide clusters and have not been observed with mononegative carbide clusters. It may be possible to limit the cluster building process by high dilution techniques or selective reagent addition, but this strategy was precluded for the synthesis of $[Ni_3Fe_3(CO)_{13}C]^{2-}$, X, by low solubility of the reactants in a common solvent.

The absence of cyclopentadiene in the cluster $[Ni_3Fe_3(CO)_{13}C]^{2-}$, X, was surprising given the general utility of $[CpNi(CO)]_2$ as a CpNi fragment source in other cluster syntheses,[19] but some precedence does exist for the observed cyclopentadiene transfer.[20] Nickelocene was identified as the other reaction product by mass spectroscopy.

Table II. Selected Bond Distances (Å) and Angles (deg) for $[PPN][RhFe_3(CO)_{12}C]\cdot CH_2Cl_2$, VIII[a]

Bond Distances

M1-M2	2.630 (2)	M1-C41	1.84 (2)
M1-Fe2	2.681 (3)	M1-C42	1.91 (2)
M1-Fe3	2.675 (3)	M1-C43	1.88 (2)
M2-Fe2	2.659 (3)	C11-O11	1.19 (2)
M2-Fe3	2.676 (3)	C12-O12	1.12 (2)
M1-C1	2.12 (1)	C13-O13	1.12 (2)
M2-C1	2.06 (1)	C21-O21	1.18 (2)
Fe2-C1	1.73 (2)	C22-O22	1.10 (2)
Fe3-C1	1.80 (2)	C23-O23	1.12 (2)
M2-C11	1.78 (2)	C31-O31	1.24 (3)
M2-C12	1.83 (2)	C32-O32	1.11 (2)
M2-C13	1.86 (2)	C33-O33	1.15 (2)
Fe2-C21	1.76 (2)	C41-O41	1.14 (2)
Fe2-C22	1.87 (2)	C42-O42	1.09 (2)
Fe2-C23	1.77 (2)	C43-O43	1.11 (2)
Fe3-C31	1.71 (3)		
Fe3-C32	1.84 (2)		
Fe3-C33	1.71 (2)		

Bond Angles

M2-M1-Fe2	60.09 (6)	C41-M1-C42	101.3 (8)
M2-M1-Fe3	60.59 (7)	C41-M1-C43	97.6 (8)
Fe2-M1-Fe3	82.21 (8)	C42-M1-C43	100.6 (7)
M1-M2-Fe2	60.90 (7)	C11-M2-C12	100.3 (7)
M1-M2-Fe3	60.55 (7)	C11-M2-C13	100.2 (7)
Fe2-M2-Fe3	82.60 (8)	C12-M2-C13	100.0 (8)
M1-Fe2-M2	59.00 (6)	C21-Fe2-C22	100.9 (9)
M1-Fe3-M2	58.86 (6)	C21-Fe2-C23	98.4 (8)
M2-M1-C1	49.9 (4)	C22-Fe2-C23	98.7 (8)
Fe2-M1-C1	40.0 (5)	C31-Fe3-C32	100.5 (8)
Fe3-M1-C1	42.2 (5)	C31-Fe3-C33	94.8 (9)
M1-M2-C1	52.0 (4)	C32-Fe3-C33	98.7 (8)
Fe2-M2-C1	40.4 (5)	M2-C11-O11	175 (2)
Fe3-M2-C1	42.3 (6)	M2-C12-O12	173 (2)
M1-Fe2-C1	52.1 (5)	M2-C13-O13	175 (2)
M2-Fe2-C1	50.7 (4)	Fe2-C21-O21	174 (2)
M1-Fe3-C1	52.1 (4)	Fe2-C22-O22	177 (2)
M2-Fe3-C1	50.2 (4)	Fe2-C23-O23	175 (2)
M1-C1-M2	78.1 (4)	Fe3-C31-O31	176 (2)
M1-C1-Fe2	87.8 (6)	Fe3-C32-O32	176 (2)
M1-C1-Fe3	85.7 (7)	Fe3-C33-O33	176 (2)
M2-C1-Fe2	88.9 (6)	M1-C41-O41	173 (2)
M2-C1-Fe3	87.6 (7)	M1-C42-O42	174 (2)
Fe2-C1-Fe3	173.2 (8)	M1-C43-O43	178 (2)

[a] Numbers in parentheses are estimated standard deviations in the least significant digits.

Scheme I

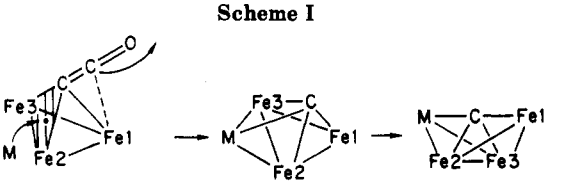

In conjunction with earlier work,[8] these results indicate that redox condensation reactions starting with $[Fe_3(CO)_9(CCO)]^{2-}$, I, provide a fairly general route to new mixed-metal butterfly carbide clusters. As illustrated by reaction 6, redox condensation may proceed beyond single metal addition. This same lack of control was observed when $[Fe_4(CO)_{12}C]^{2-}$, II, underwent the addition of two heterometal atoms to yield hexanuclear clusters.[7] The multiple metal addition reactions occur in some syntheses of dinegative carbide clusters and have not been observed with mononegative carbide clusters. It may be possible to limit the cluster building process by high dilution techniques or selective reagent addition, but this strategy was precluded for the synthesis of $[Ni_3Fe_3(CO)_{13}C]^{2-}$, X, by low solubility of the reactants in a common solvent.

The absence of cyclopentadiene in the cluster $[Ni_3Fe_3(CO)_{13}C]^{2-}$, X, was surprising given the general utility of $[CpNi(CO)]_2$ as a CpNi fragment source in other cluster syntheses,[19] but some precedence does exist for the observed cyclopentadiene transfer.[20] Nickelocene was identified as the other reaction product by mass spectroscopy.

All of the heterometallic butterfly carbides that have been isolated and characterized to date (VIa,b, VIII, and IX) have the heterometal at a hinge site. The reasons for this site preference are still not clear. On the basis of analogy with the reactions of $[Fe_3(CO)_9(CCO)]^{2-}$, I, with small electrophiles and steric considerations,[2] the expected site of attack of I is on the ketenyl face. As illustrated in

(19) For example: (a) Hsieh, A. T. T.; Knight, J. *J. Organomet. Chem.* **1971**, *26*, 125. (b) Raverdino, V.; Aime, S.; Milone, L.; Sappa, E. *Inorg. Chim. Acta* **1978**, *30*, 9. (c) Sappa, E.; Lanfranchi, M.; Tiripicchio, A.; Camellini, M. T. *J. Chem. Soc., Chem. Commun.* **1981**, 995. (d) Shore, S. G.; Hsu, W. L.; Weisenberger, C. R.; Caste, M. L.; Churchill, M. R.; Bueno, C. *Organometallics* **1982**, *1*, 1405.

(20) Lanfranchi, M.; Tiripicchio, A.; Sappa, E.; MacLaughlin, S. A.; Carty, A. J. *J. Chem. Soc., Chem. Commun.* **1982**, 538.

Table III. Positional Parameters and Their Estimated Standard Deviations for [PPN][$RhFe_3(CO)_{12}C$]·CH_2Cl_2, VIII

atom	x	y	z	atom	x	y	z
Cl91	0.7673 (7)	0.5570 (6)	0.865 (1)	C112	0.6927 (8)	0.1325 (8)	0.781 (1)
Cl92	0.8330 (6)	0.6158 (8)	0.736 (2)	C113	0.733 (1)	0.1280 (9)	0.860 (1)
M1	0.51697 (8)	0.54522 (7)	0.750	C114	0.743 (1)	0.1845 (9)	0.908 (1)
M2	0.4540 (1)	0.54578 (8)	0.5929 (1)	C115	0.712 (1)	0.248 (1)	0.887 (1)
Fe2	0.5758 (1)	0.6214 (1)	0.6204 (2)	C116	0.6717 (9)	0.2544 (8)	0.804 (1)
Fe3	0.3972 (1)	0.6245 (1)	0.7208 (2)	C121	0.6686 (8)	0.2426 (7)	0.572 (1)
C1	0.488 (1)	0.6279 (6)	0.667 (1)	C122	0.7097 (8)	0.2045 (8)	0.513 (1)
C11	0.516 (1)	0.4846 (9)	0.546 (1)	C123	0.757 (1)	0.233 (1)	0.456 (1)
C12	0.421 (1)	0.589 (1)	0.493 (1)	C124	0.7643 (9)	0.306 (1)	0.460 (1)
C13	0.3712 (9)	0.4911 (8)	0.617 (1)	C125	0.723 (1)	0.345 (1)	0.514 (1)
C21	0.627 (1)	0.676 (1)	0.690 (1)	C126	0.6765 (9)	0.3120 (7)	0.575 (1)
C22	0.654 (1)	0.5686 (9)	0.573 (1)	C131	0.5262 (7)	0.2471 (7)	0.669 (1)
C23	0.562 (1)	0.6779 (8)	0.531 (1)	C132	0.4943 (8)	0.2763 (8)	0.595 (1)
C31	0.410 (1)	0.6811 (9)	0.805 (2)	C133	0.4200 (9)	0.3073 (9)	0.608 (1)
C32	0.3180 (9)	0.5744 (9)	0.765 (1)	C134	0.3881 (9)	0.3110 (9)	0.689 (1)
C33	0.347 (1)	0.6800 (9)	0.656 (1)	C135	0.4228 (9)	0.2848 (9)	0.764 (1)
C41	0.5927 (9)	0.4842 (8)	0.726 (1)	C136	0.4946 (8)	0.2513 (7)	0.752 (1)
C42	0.558 (1)	0.5929 (9)	0.849 (1)	C211	0.5668 (9)	−0.0118 (6)	0.611 (1)
C43	0.451 (1)	0.485 (1)	0.807 (1)	C212	0.6452 (8)	−0.0185 (8)	0.591 (1)
O11	0.5531 (8)	0.4398 (7)	0.5153 (9)	C213	0.672 (1)	−0.0859 (9)	0.583 (1)
O12	0.3976 (9)	0.6090 (8)	0.430 (1)	C214	0.630 (1)	−0.1420 (8)	0.594 (1)
O13	0.3205 (6)	0.4578 (6)	0.625 (1)	C215	0.552 (1)	−0.1345 (9)	0.615 (1)
O21	0.6546 (8)	0.7159 (6)	0.738 (1)	C216	0.522 (1)	−0.0676 (9)	0.623 (1)
O22	0.6995 (8)	0.5358 (6)	0.548 (1)	C221	0.4790 (7)	0.0796 (7)	0.503 (1)
O23	0.550 (1)	0.7159 (8)	0.478 (1)	C222	0.417 (1)	0.0351 (9)	0.488 (1)
O31	0.4248 (9)	0.7227 (7)	0.864 (1)	C223	0.3816 (9)	0.043 (1)	0.406 (1)
O32	0.2711 (7)	0.5458 (8)	0.796 (1)	C224	0.4061 (9)	0.090 (1)	0.345 (1)
O33	0.3149 (9)	0.7150 (7)	0.608 (1)	C225	0.465 (1)	0.135 (1)	0.361 (1)
O41	0.6387 (8)	0.4441 (6)	0.7199 (9)	C226	0.5029 (9)	0.1265 (9)	0.441 (1)
O42	0.5850 (8)	0.6225 (8)	0.901 (1)	C231	0.4620 (8)	0.0814 (7)	0.695 (1)
O43	0.4146 (8)	0.4479 (7)	0.841 (1)	C232	0.486 (1)	0.0654 (9)	0.781 (1)
P1	0.6105 (2)	0.1985 (2)	0.6519 (3)	C233	0.436 (1)	0.078 (1)	0.850 (1)
P2	0.5287 (2)	0.0727 (2)	0.6077 (3)	C234	0.364 (1)	0.107 (1)	0.838 (2)
N1	0.5962 (6)	0.1260 (5)	0.6166 (9)	C235	0.342 (1)	0.123 (1)	0.746 (2)
C111	0.6621 (7)	0.1938 (8)	0.757 (1)	C236	0.3890 (8)	0.1127 (9)	0.679 (1)

Table IV. Selected Bond Distances (Å) and Angles (deg) for [PPN][$CoFe_4(CO)_{14}C$], XI[a]

Bond Distances

M5-M1	2.533 (1)	M3-C31	1.785 (7)	M3-C1	1.870 (5)	C31-O31	1.139 (6)
M5-M3	2.643 (1)	M3-C32	1.780 (7)	M4-C1	1.962 (5)	C32-O32	1.152 (7)
M5-M4	2.572 (1)	M3-C33	1.756 (7)	M5-C51	1.977 (6)	C33-O33	1.147 (6)
M1-M2	2.626 (1)	M4-C41	1.759 (6)	M5-C52	1.758 (6)	C41-O41	1.161 (6)
M1-M4	2.575 (1)	M4-C42	1.755 (7)	M5-C53	1.801 (6)	C42-O42	1.155 (7)
M2-M3	2.666 (1)	M4-C43	1.770 (7)	M1-C12	1.782 (6)	C43-O43	1.138 (7)
M2-M4	2.630 (1)	C12-O12	1.144 (6)	M1-C13	1.749 (6)	C51-O51	1.147 (6)
M3-M4	2.581 (1)	C13-O13	1.150 (6)	M1-C51	1.962 (6)	C52-O52	1.145 (6)
M5-C1	1.854 (5)	C21-O21	1.135 (6)	M2-C21	1.792 (6)	C53-O53	1.126 (6)
M1-C1	1.865 (5)	C22-O22	1.142 (6)	M2-C22	1.785 (7)		
M2-C1	1.838 (5)	C23-O23	1.156 (7)	M2-C23	1.751 (7)		

Bond Angles

M1-M5-M3	91.78 (3)	M5-C1-M4	84.7 (2)	M3-M5-C1	45.0 (2)	C41-M4-C42	89.1 (3)
M1-M5-M4	60.58 (3)	M1-C1-M2	90.3 (2)	M4-M5-C1	49.4 (2)	C41-M4-C43	96.0 (3)
M3-M5-M4	59.31 (3)	M1-C1-M3	168.9 (3)	M5-M1-C1	46.9 (1)	C42-M4-C43	96.1 (3)
M5-M1-M2	91.05 (4)	M1-C1-M4	84.6 (2)	M2-M1-C1	44.4 (1)	M1-C12-O12	178.6 (5)
M5-M1-M4	60.45 (3)	M2-C1-M3	91.9 (2)	M4-M1-C1	49.3 (2)	M1-C13-O13	178.1 (6)
M2-M1-M4	60.75 (3)	M2-C1-M4	87.6 (2)	M1-M2-C1	45.3 (2)	M2-C21-O21	178.3 (7)
M1-M2-M3	89.25 (3)	M3-C1-M4	84.7 (2)	M3-M2-C1	44.5 (2)	M2-C22-O22	172.4 (6)
M1-M2-M4	58.68 (3)	C51-M5-C52	97.5 (3)	M4-M2-C1	48.2 (2)	M2-C23-O23	176.5 (6)
M3-M2-M4	58.33 (3)	C51-M5-C53	96.5 (3)	M5-M3-C1	44.5 (1)	M3-C31-O31	172.4 (7)
M5-M3-M2	87.83 (3)	C52-M5-C53	101.3 (3)	M2-M3-C1	43.6 (1)	M3-C32-O32	177.4 (7)
M5-M3-M4	58.97 (3)	C12-M1-C13	98.1 (3)	M4-M3-C1	49.2 (2)	M3-C33-O33	175.2 (6)
M2-M3-M4	60.15 (3)	C12-M1-C51	97.2 (3)	M5-M4-C1	45.9 (1)	M4-C41-O41	176.6 (6)
M5-M4-M1	58.97 (3)	C13-M1-C51	93.2 (3)	M1-M4-C1	46.1 (2)	M4-C42-O42	173.5 (7)
M5-M4-M2	90.11 (3)	C21-M2-C22	99.6 (3)	M2-M4-C1	44.3 (1)	M4-C43-O43	172.7 (7)
M5-M4-M3	61.72 (3)	C21-M2-C23	97.3 (3)	M3-M4-C1	46.2 (2)	M5-C51-O51	139.8 (5)
M1-M4-M2	60.58 (3)	C22-M2-C23	95.1 (3)	M5-C1-M1	85.9 (2)	M1-C51-O51	140.1 (5)
M1-M4-M3	92.27 (4)	C31-M3-C32	97.5 (3)	M5-C1-M2	171.7 (3)	M5-C52-O52	177.6 (6)
M2-M4-M3	61.52 (3)	C31-M3-C33	94.1 (3)	M5-C1-M3	90.4 (2)	M5-C53-O53	178.3 (6)
M1-M5-C1	47.3 (2)	C32-M3-C33	99.5 (3)				

[a] Numbers in parentheses are estimated standard deviations in the least significant digits.

Scheme I, attack at this site should lead to the placement of the heterometal at a wingtip. Initial attack of the electrophile on the opposite face of I (Scheme II) to form a capped tetrahedron should readily lead to the butterfly configuration having the heterometal on the hinge. It is also possible that the initial reaction follows Scheme I, but

Table V. Positional Parameters and Their Estimated Standard Deviations for $[PPN][CoFe_4(CO)_{14}C]$, XI

atom	x	y	z	atom	x	y	z
M5	0.87233 (5)	0.43626 (5)	0.22382 (4)	C111	1.3240 (3)	0.4903 (3)	0.2529 (3)
M1	0.82823 (5)	0.52491 (5)	0.11017 (4)	C112	1.3665 (4)	0.4757 (4)	0.2019 (3)
M2	0.68596 (5)	0.45679 (6)	0.07827 (5)	C113	1.4157 (4)	0.5367 (5)	0.1875 (3)
M3	0.72964 (5)	0.36775 (5)	0.20055 (5)	C114	1.4222 (4)	0.6112 (4)	0.2228 (4)
M4	0.74712 (5)	0.52773 (5)	0.20527 (4)	C115	1.3796 (4)	0.6276 (4)	0.2713 (4)
C1	0.7797 (3)	0.4388 (3)	0.1485 (3)	C116	1.3300 (3)	0.5663 (4)	0.2858 (3)
C12	0.8294 (3)	0.6346 (4)	0.0951 (3)	C121	1.3321 (3)	0.3271 (4)	0.3205 (3)
C13	0.8653 (4)	0.4928 (4)	0.0377 (3)	C122	1.4135 (3)	0.3345 (4)	0.3357 (3)
C21	0.5818 (4)	0.4414 (4)	0.0692 (4)	C123	1.4608 (4)	0.2685 (5)	0.3671 (4)
C22	0.6808 (4)	0.5432 (4)	0.0182 (3)	C124	1.4281 (4)	0.1967 (4)	0.3833 (4)
C23	0.6966 (4)	0.3816 (4)	0.0149 (3)	C125	1.3481 (4)	0.1888 (4)	0.3708 (4)
C31	0.7819 (4)	0.3340 (4)	0.2897 (3)	C126	1.2994 (4)	0.2541 (4)	0.3378 (3)
C32	0.6313 (4)	0.3539 (4)	0.2098 (4)	C131	1.2022 (3)	0.3649 (4)	0.1956 (3)
C33	0.7414 (4)	0.2724 (4)	0.1593 (3)	C132	1.2302 (3)	0.3054 (4)	0.1562 (3)
C41	0.8130 (3)	0.6097 (4)	0.2412 (3)	C133	1.1822 (4)	0.2749 (4)	0.0923 (3)
C42	0.6609 (4)	0.5863 (4)	0.1673 (4)	C134	1.1050 (4)	0.3008 (5)	0.0681 (3)
C43	0.7229 (4)	0.5032 (4)	0.2874 (3)	C135	1.0773 (4)	0.3603 (5)	0.1059 (3)
C51	0.9328 (3)	0.5172 (4)	0.1810 (3)	C136	1.1246 (3)	0.3915 (4)	0.1697 (3)
C52	0.9279 (3)	0.3470 (4)	0.2154 (3)	C211	1.2995 (3)	0.4558 (4)	0.4723 (3)
C53	0.9159 (4)	0.4644 (4)	0.3174 (3)	C212	1.3500 (3)	0.5237 (4)	0.4884 (3)
O12	0.8314 (3)	0.7051 (3)	0.0867 (2)	C213	1.4225 (4)	0.5155 (5)	0.5392 (4)
O13	0.8879 (3)	0.4701 (3)	−0.0105 (2)	C214	1.4444 (4)	0.4412 (6)	0.5726 (4)
O21	0.5159 (2)	0.4297 (4)	0.0626 (3)	C215	1.3959 (4)	0.3746 (5)	0.5561 (4)
O22	0.6690 (3)	0.5959 (3)	−0.0236 (3)	C216	1.3231 (3)	0.3803 (4)	0.5060 (3)
O23	0.7078 (3)	0.3322 (3)	−0.0255 (3)	C221	1.1380 (3)	0.3917 (3)	0.4296 (3)
O31	0.8080 (3)	0.3074 (3)	0.3464 (2)	C222	1.0934 (3)	0.3365 (4)	0.3796 (3)
O32	0.5689 (3)	0.3446 (3)	0.2186 (3)	C223	1.0400 (3)	0.2837 (4)	0.3994 (3)
O33	0.7547 (3)	0.2113 (3)	0.1335 (2)	C224	1.0303 (3)	0.2866 (4)	0.4677 (3)
O41	0.8577 (3)	0.6615 (3)	0.2681 (2)	C225	1.0729 (4)	0.3416 (5)	0.5179 (3)
O42	0.6048 (3)	0.6276 (3)	0.1489 (3)	C226	1.1267 (4)	0.3943 (4)	0.4988 (3)
O43	0.7094 (3)	0.4958 (3)	0.3423 (3)	C231	1 1671 (3)	0.5659 (3)	0.4062 (3)
O51	0.9960 (2)	0.5436 (3)	0.1912 (2)	C232	1.1224 (3)	0.6011 (4)	0.3414 (3)
O52	0.9617 (3)	0.2874 (3)	0.2090 (2)	C233	1.0869 (3)	0.6773 (4)	0.3404 (3)
O53	0.9414 (3)	0.4827 (3)	0.3760 (2)	C234	1.0966 (3)	0.7207 (4)	0.4038 (3)
P1	1.26470 (8)	0.4088 (1)	0.27755 (8)	C235	1.1408 (3)	0.6888 (4)	0.4684 (3)
P2	1.20535 (8)	0.4624 (1)	0.40396 (7)	C236	1.1746 (3)	0.6116 (4)	0.4700 (3)
N1	1.2098 (2)	0.4430 (3)	0.3239 (2)				

Scheme II

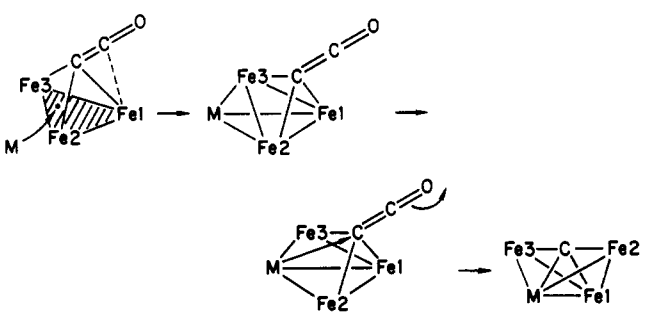

the cluster rearranges to a more stable form.

Recently, $[CoFe_2(CO)_9(CCO)]^-$ was synthesized from $[Fe_3(CO)_9(CCO)]^{2-}$ and $Co_2(CO)_8$ via a metal substitution reaction (eq 8).[8] This observation along with similar

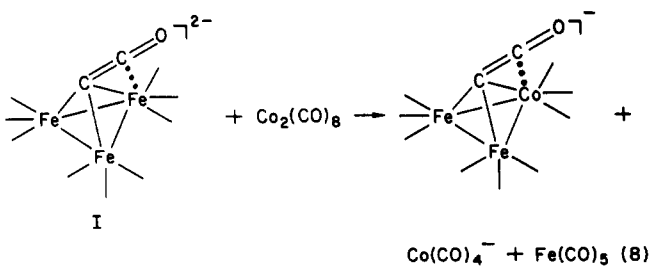

I

$$Co(CO)_4^- + Fe(CO)_5 \quad (8)$$

reactions[21] prompted us to attempt the generation of $[CoFe_3(CO)_{12}C]^-$ by the reaction of $[Fe_4(CO)_{12}C]^{2-}$, II, with a stoichiometric amount of $Co_2(CO)_8$. Initially it appeared that a metal substitution had occurred because both $Co(CO)_4^-$ and $Fe(CO)_5$ were detected as reaction products. However, the cluster product that has been isolated and characterized is the pentanuclear cluster $[CoFe_4(CO)_{14}C]^-$, XI (eq 9). The $Fe(CO)_5$ detected presumably arises from cluster decomposition.

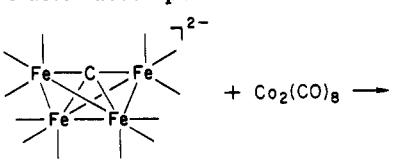

II

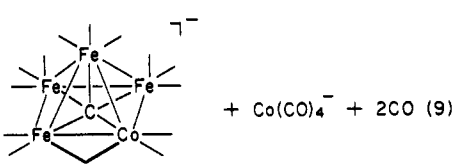

XI (Co position arbitrary)

Metal substitution reactions are gaining increasing utility in the syntheses of carbonyl clusters,[21] but it is still not possible to predict the course of these reactions with great certainty. The substitution reactions with $Co_2(CO)_8$ are thought to proceed via radical pathways involving heterometal addition followed by metal extrusion.[21a] In some cases the carbide radical may be sufficiently stable to resist the extrusion step. In this connection, the carbide ligand may stabilize the intermediate cluster and thus promote the cluster building pathway.[22-24]

(21) (a) Horwitz, C. P.; Holt, E. M.; Shriver, D. F., manuscript in preparation. (b) Beurich, H.; Blumhofer, R.; Vahrenkamp, H. *Chem. Ber.* **1982**, *115*, 2409. (c) Epstein, R. A.; Withers, H. W.; Geoffroy, G. L. *Inorg. Chem.* **1979**, *18*, 942. (d) Ceriotti, A.; Longoni, G.; Pergola, R. D.; Heaton, B. T.; Smith, D. O. *J. Chem. Soc., Dalton Trans.* **1983**, 1433.

(22) Kolis, J. W.; Basolo, F.; Shriver, D. F. *J. Am. Chem. Soc.* **1982**, *104*, 5626.

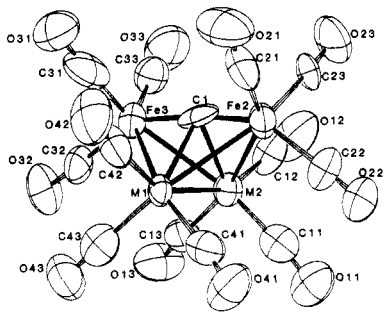

Figure 1. ORTEP drawing of the cluster unit in $[PPN][RhFe_3(CO)_{12}C]\cdot CH_2Cl_2$, VIII, with thermal ellipsoids drawn at the 50% probability level.

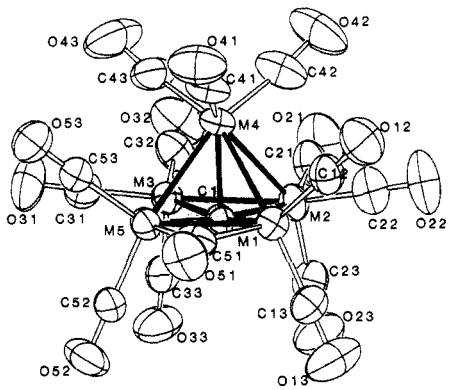

Figure 2. ORTEP drawing of the cluster unit in $[PPN][CoFe_4(CO)_{14}C]$, XI, with thermal ellipsoids drawn at the 50% probability level. The Co atom was arbitrarily refined in the position labeled M5.

X-ray Crystal Structure of $[PPN][RhFe_3(CO)_{12}C]\cdot CH_2Cl_2$, VIII. As with all previously characterized tetranuclear carbide clusters, VIII adopts a butterfly metal core arrangement with the carbide located between the wingtip metals and centered over the hinge metal–metal bond (Figure 1). As with VIb the heterometal is located selectively at a hinge position.[8] Each of the metals bears three terminal carbonyls (Fe–C(av) = 1.78 Å; M–C(av) = 1.85 Å; C–O(av) = 1.14 Å) with no bridging or semibridging interactions. The average metal–metal distance of 2.66 Å is slightly larger than that of the related clusters $[Fe_4(CO)_{12}C]^{2-}$, II, and $[HFe_4(CO)_{12}C]^-$, III, which have average iron–iron distances of 2.62 Å.[3b,4] This increase is expected because of the presence of the second-row rhodium atom in the cluster. Another effect of the rhodium atom in the cluster is the distortion of the metal–carbide bond lengths in comparison with homometallic butterfly carbides. For II, III, and $Fe_4(CO)_{13}C$, IV, the $Fe_{wingtip}$–$C_{carbide}$ distances average 1.79 Å and the Fe_{hinge}–$C_{carbide}$ distances range from 1.94 to 1.99 Å. In contrast, the $Fe_{wingtip}$–$C_{carbide}$ distance in VIII averages 1.76 Å and the M_{hinge}–$C_{carbide}$ averages 2.09 Å. This distortion is clearly demonstrated by the small dihedral angle of 98° in VIII in comparison with 101, 104, and 101° for II, III, and IV, respectively. These distortions may be a factor in determining the reactivity of this cluster.

X-ray Crystal Structures of $[PPN][CoFe_4(CO)_{14}C]$, XI. As shown in the ORTEP diagram (Figure 2), this compound adopts a square-pyramidal metal framework with approximate C_s symmetry. The carbide carbon is approximately equidistant from the four basal metals and is situated 0.15 Å out of the least-squares basal plane toward the side away from the apical metal. This metal framework is predicted for this 74-electron cluster and has also been found in the isoelectronic $Fe_5(CO)_{15}C$, XIV,[23] $[Fe_5(CO)_{14}C]^{2-}$, XV,[25] and $[RhFe_4(CO)_{14}C]^-$, XVI.[7a] There is one bridging carbonyl between M5 and M1 with each of these metals also bearing two terminal carbonyls and three terminal carbonyls on each of the other three metals. The metal–metal nonbridged distances average 2.61 Å, which compares well with the average iron–iron distances of 2.64 Å in XIV, 2.61 Å in XV, and 2.62 Å in XVI. As usual, the carbonyl-bridged M1–M5 distance of 2.533 (1) Å is considerably shorter than that of the nonbridged metal–metal bonds. In all four structures, XI, XIV, XV, and XVI, the carbide carbon is within bonding distance of all five metal atoms with the apical metal always further away (for XI, average M_{bas}–C = 1.86 Å, M_{ap}–C = 1.96 Å; for XIV, average Fe_{bas}–C = 1.88 Å, Fe_{ap}–C = 1.96 Å; for XV, average Fe_{bas}–C = 1.87 Å, Fe_{ap}–C = 2.01 Å; for XVI, average M_{bas}–C = 1.90 Å, M_{ap}–C = 1.98 Å). This longer M–$C_{carbide}$ distance reflects the fact that in all three cases the carbide sits out of the basal plane away from the apical metal. The magnitude of this displacement increases significantly from the neutral homonuclear cluster XIV to the anionic XI, XV, and XVI (0.08, 0.15, 0.18, and 0.19 Å, respectively), and it has been postulated that it is due to the increase in charge on the metal carbide skeleton.[25]

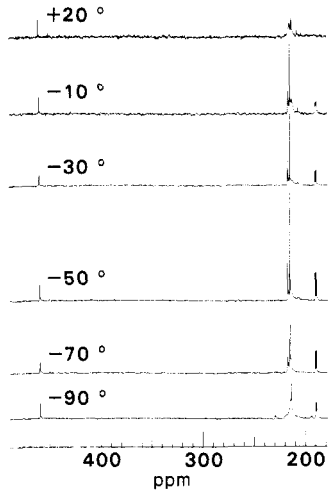

Figure 3. Variable-temperature ^{13}C NMR spectra of the downfield region of a CD_2Cl_2 solution of $[PPN][RhFe_3(CO)_{12}C]\cdot CH_2Cl_2$, VIII.

^{13}C NMR Studies. Variable-temperature ^{13}C NMR spectroscopy was a valuable aid in both product characterization and solution structure determination of the mixed-metal carbide species. $[Fe_3(CO)_9(CCO)]^{2-}$, I, that has been ^{13}C enriched at all carbons is readily prepared by the reductive cleavage route (eq 1) starting with ^{13}C-enriched $[Fe_3(CO)_{11}]^{2-}$. This ^{13}C-enriched sample of I yields mixed-metal carbide species enriched at both the carbide and carbonyl carbons. The resulting enrichment at all carbons allows facile interpretation of fluxionality patterns because the carbide resonance is generally temperature independent and thereby acts as a useful internal standard, although care must be exercised in intensity measurements due to the introduction of ^{12}CO from the electrophile. The solution structures of the butterfly carbides $[RhFe_3(CO)_{12}C]^-$, VIII, and $[MnFe_3(CO)_{13}C]^-$, IX, are readily elucidated by their ^{13}C NMR spectra. For the higher order clusters $[Ni_3Fe_3(CO)_{13}C]^{2-}$, X, and $[CoFe_4(CO)_{14}C]^-$, XI, solution structure assignments were not

(23) Braye, E. H.; Dahl, L. F.; Hübel, W.; Wampler, D. L. *J. Am. Chem. Soc.* **1962**, *84*, 4633.
(24) (a) Wijeyesekera, S. D.; Hoffmann, R.; Wilker, C. N. *Organometallics* **1984**, *3*, 962. (b) Harris, S.; Bradley, J. S. *Organometallics* **1984**, *3*, 1086.
(25) Gourdon, A.; Jeannin, Y. *C. R. Acad. Sci Paris, Series II* **1983**, *295*, 1101.

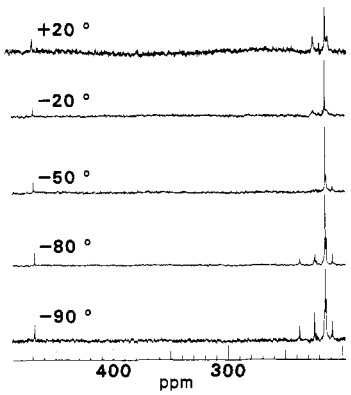

Figure 4. Variable-temperature ^{13}C NMR spectra of the downfield region of a CD_2Cl_2 solution of [PPN][$MnFe_3(CO)_{13}C$], IX.

achieved owing in part to the lack of significant change in the spectra over the temperature range studied (+30 to -90 °C).

Figure 3 shows the variable-temperature ^{13}C NMR spectra of a CD_2Cl_2 solution of [$RhFe_3(CO)_{12}C$]$^-$, VIII. This compound displays the characteristic downfield chemical shift of a carbide, 461.1 ppm, which is a doublet with $^1J_{Rh-C}$ = 19.5 Hz. The magnitude of this coupling constant is typical in rhodium carbide clusters.[26] Consistent with the solid-state structure (Figure 1), all of the carbonyl resonances are in the downfield region typical of terminal carbonyls, approximately 230–180 ppm.

The room-temperature spectrum shows several broad and overlapping resonances at approximately 215 ppm for the 12 carbonyls. As the temperature is lowered these resonances form a distinct pattern of three peaks and the upfield component is a doublet owing to coupling with the rhodium ($^1J_{Rh-C}$ = 63.5 Hz). These peaks sharpen and increase in intensity down to -50 °C, where the integrated intensities are approximately 3:6:3 vs. the carbide resonance. Upon further cooling, the carbonyl peaks lose intensity and broaden. The -50 °C spectrum is consistent with a butterfly cluster having C_s symmetry and with three terminal carbonyls per metal, assuming the system is undergoing rapid intrasite carbonyl exchange. Rapid intrasite exchange is common in this type of cluster and is seen, for example, in the low-temperature ^{13}C NMR spectra of [$Fe_4(CO)_{12}C$]$^{2-}$, II,[3a] and [$HFe_4(CO)_{12}C$]$^-$, III.[3b] C_s symmetry is consistent with a structure having the rhodium at either the hinge or wingtip site. The X-ray crystal structure confirms that the rhodium occupies a hinge site and the cluster has near C_s symmetry in the solid state.

The variable-temperature ^{13}C NMR spectra of [$MnFe_3(CO)_{13}C$]$^-$, IX (Figure 4), displays a temperature-independent downfield resonance for the carbide at 468.4 ppm. At -20 °C the carbonyl region of the spectrum displays several broad resonances around 217 ppm and one sharp resonance at 215.3 ppm. Upon cooling to -50 °C the peak at 215 ppm increases in intensity while the rest remain broad. From -50 to -80 °C this peak integrates as ca. six carbonyls vs. the carbide resonance, implying the fluxional process relating the six carbonyls is at a temperature limit. Upon further cooling to -90 °C this resonance begins to decrease in intensity. The rest of the carbonyl resonances consist of four peaks at 238, 224, 214, and 209 ppm with approximate intensities of 1:3:2:1 at -90 °C. These appear to all be involved in the same fluxionality process and have not yet reached the low-temperature limit at -90 °C. The peak at 238 ppm is assigned to a bridging carbonyl, and the remaining three peaks are associated with six terminal carbonyls.

This 62-electron butterfly carbide can exist in either two forms. The manganese may occur a hinge site as was found for [$MFe_3(CO)_{13}C$]$^{2-}$ (VIa,b, M = Cr, W) and VIII, or it may occupy a wingtip site. As described below, an argument based on physically reasonable assumptions and the NMR data leads us to prefer a hinge site for the Mn atom.

It is assumed that the group 7 manganese will be bonded to the extra carbonyl (i.e., the bridging carbonyl) in order to come closest to satisfying the EAN rule and that all four metals will bear three terminal carbonyls. It is also postulated that only intrasite carbonyl exchange occurs at low temperature, a result consistent with all reported variable-temperature ^{13}C NMR spectra for butterfly carbide clusters II, III, and VIII. If the manganese occupies a wingtip site, the bridging carbonyl must bridge a wingtip–hinge metal–metal bond. The cluster would have no symmetry, and this appears to be inconsistent with the ^{13}C NMR spectra. If the manganese occupies a hinge site, the bridging carbonyl could bridge the hinge bond, thereby giving the cluster C_s symmetry. The resonance at 215 ppm would then be assigned to the carbonyls on the wingtip irons that are undergoing rapid intramolecular scrambling and are related by the mirror plane. Thus the solution structure is probably analogous to $Fe_4(CO)_{13}C$, IV, with the manganese at a hinge site.

Reactivity with Proton Sources. Protonation is a useful probe for carbide reactivity. For example, [$Fe_4(CO)_{12}C$]$^{2-}$, II, is known to react with excess acid to yield the methylidyne cluster $HFe_4(CO)_{12}(CH)$, V (eq 10), which

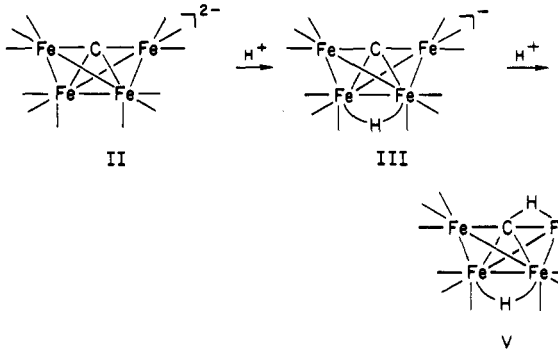

II III V (10)

is readily characterized by ^1H and ^{13}C NMR spectroscopy.[3a] Similarly the mixed-metal butterfly carbide [$WFe_3(CO)_{13}C$]$^{2-}$, VIb, is known to react with excess acid to generate $HWFe_3(CO)_{13}(CH)$, VII (eq 11).[8]

$$[WFe_3(CO)_{13}C]^{2-} + 2H^+ \rightarrow HWFe_3(CO)_{13}(CH) \quad (11)$$
VIb VII

When a CH_2Cl_2 solution of VIII is treated with 1 equiv of HSO_3CF_3 at -90 °C, the tetranuclear methylidyne cluster $RhFe_3(CO)_{12}(CH)$, XII, is generated as judged by ^1H and ^{13}C NMR (eq 12). This cluster displays a char-

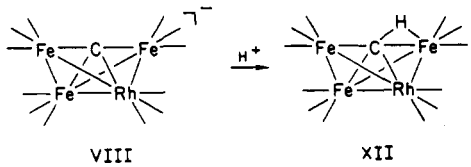

VIII XII (12)

acteristic upfield resonance in the ^1H NMR spectra at -1.48 ppm and a downfield resonance in the ^{13}C NMR at 340 ppm with $^1J_{C-H}$ = 102 Hz. Unfortunately, the methyne

(26) (a) Albano, V. G.; Chini, P.; Martinengo, S.; McCaffrey, D. J. A.; Strumolo, D.; Heaton, B. T. *J. Am. Chem. Soc.* **1974**, *96*, 8106. (b) Heaton, B. T.; Strona, L.; Martinengo, S.; Strumolo, D.; Goodfellow, R. J.; Sadler, I. H. *J. Chem. Soc., Dalton Trans.* **1982**, 1499. (c) Heaton, B. T.; Strona, L.; Martinengo, S.; Strumolo, D.; Albano, V. G.; Braga, D. *J. Chem. Soc., Dalton Trans.* **1983**, 2175.

cluster is unstable and decomposes even at −90 °C. One of the decomposition products is $HFe_3(CO)_{10}(CH)$ as judged by NMR,[2] but the nature of the other products is not yet known.

When a CH_2Cl_2 solution of $[MnFe_3(CO)_{13}C]^-$, IX, is treated with a slight excess of HSO_3CF_3, the methylidyne cluster $MnFe_3(CO)_{13}(CH)$, XIII, is generated (eq 13). In

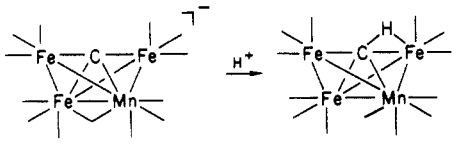

IX XIII (13)

contrast to XII, this cluster may be isolated and characterized. This cluster has characteristic resonances for the methylidyne moiety at −0.33 ppm in the ^1H NMR spectrum and 336 ppm in the ^{13}C NMR spectrum, with $^1J_{C-H}$ = 107 Hz.

The protonation of a metal–carbon bond in $[RhFe_3(CO)_{12}C]^-$, VIII, and $[MnFe_3(CO)_{13}C]^-$, IX (eq 12 and 13), contrasts with the protonation of $[Fe_4(CO)_{12}C]^{2-}$, II, for which the first equivalent adds across the iron–iron hinge bond to yield $[HFe_4(CO)_{12}C]^-$, III, and this subsequently reacts with the second equivalent of acid to generate $HFe_4(CO)_{12}(CH)$, V (eq 10). Initial protonation of the hinge metal–metal bond of II in reaction 10 is in harmony with the calculated concentration of electron density at this site.[24]

In the case of reaction 13, protonation may occur preferentially at the Fe–C bond because the hinge site is occupied by an electron-withdrawing bridging CO ligand. By contrast, the crystal structure of VIII (Figure 1) clearly indicates that the hinge position is readily accessible to a proton, and furthermore one might expect that the higher basicity of second-row metals over that of first-row metals would promote protonation at the hinge. It appears that in comparison with the dinegative cluster II, the electronic distribution in the nonnegative cluster VIII results in lower electron density on the hinge relative to the C–Fe(wingtip).

In summary, this work clearly demonstrates the utility of I in redox condensation cluster building reactions. The isolated products will be tetranuclear butterfly carbide clusters if the proper choice of reagents is employed. These new tetranuclear carbide clusters display reactivity at the carbide, and they do not undergo protonation of the metal framework as was previously seen in the homometallic butterfly carbide $[Fe_4(CO)_{12}C]^{2-}$ (II).

Acknowledgment. This research was supported by the NSF through Grant CHE-8204401. The X-ray equipment used in this research was acquired through NSF Grant CHE-8300958 and NIH Grant 1510KR01672-01. The NMR spectrometer was purchased in part from NSF Grant CHE-8015490.

Registry No. I·2PPN, 88690-38-4; I·2(Ph_4P), 93110-67-9; II, 74792-04-4; VIII·PPN, 93110-69-1; VIII·PPN·CH_2Cl_2, 93110-70-4; IX·(Ph_4P), 93110-72-6; IX·PPN, 93110-75-9; XII, 93110-73-7; XIII, 93110-74-8; $[PPN][Rh(CO)_2Cl_2]$, 89654-69-3; $[Rh(CO)_2Cl]_2$, 14523-22-9; $[Mn(CO)_5(CH_3CN)][PF_6]$, 37504-44-2; $[CpNi(CO)]_2$, 12170-92-2; $Co_2(CO)_8$, 10210-68-1; $Ni(CO)_4$, 13463-39-3; $HFe_3(CO)_{10}(CH)$, 87698-64-4.

Supplementary Material Available: Tables of positional parameters, bond lengths, bond angles, anisotropic thermal parameters, and observed and calculated structure factors for $[PPN][RhFe_3(CO)_{12}C]\cdot CH_2Cl_2$ and $[PPN][CoFe_4(CO)_{14}C]$ (109 pages). Ordering information is given on any current masthead page.

(27) **Note Added in Proof.** $[Et_4N][CoFe_4(CO)_{14}C]$ has been synthesized via a metal substitution reaction between $[Et_4N]_2[Fe_5(CO)_{14}C]$ and $CoCl_2$: Lopatin, V. E.; Mikova, N. M.; Gubin, S. P. *Izv. Akad. Nauk SSSR, Ser. Khim.* **1983**, *32*, 2170.